Conjugated donor-acceptor (D-A) supramolecule catalyst for visible-light-driven photocatalytic removal of bromate in water

Liu, Guoshuai; You, Shijie; Zhang, Yujian; Huang, Hong; Spanjers, Henri

DOI
10.1016/j.jcis.2019.06.072

Publication date
2019

Document Version
Final published version

Published in
Journal of Colloid and Interface Science

Journal of Colloid and Interface Science 553 (2019) 666–673

Contents lists available at ScienceDirect

Journal of Colloid and Interface Science

journal homepage: www.elsevier.com/locate/jcis

Regular Article

Conjugated donor-acceptor (D-A) supramolecule catalyst for visible-light-driven photocatalytic removal of bromate in water

Guoshuai Liu [a,b], Shijie You [a,*], Yujian Zhang [c], Hong Huang [a], Henri Spanjers [b]

[a] State Key Laboratory of Urban Water Resource and Environment, School of Environment, Harbin Institute of Technology, Harbin 150090, PR China
[b] Department of Water Management, Section Sanitary Engineering, Delft University of Technology, PO Box 5048, 2600 GA Delft, the Netherlands
[c] Department of Materials Chemistry, Huzhou University, Huzhou 313000, PR China

GRAPHICAL ABSTRACT

Effective bromate removal by supramolecule BDTD photocatalyst.

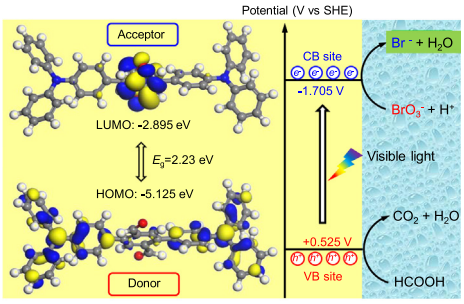

ARTICLE INFO

Article history:
Received 10 April 2019
Revised 19 June 2019
Accepted 21 June 2019
Available online 21 June 2019

Keywords:
Bromate
BDTD supramolecule
Photocatalyst
Visible light

ABSTRACT

To guarantee drinking water security, removal of bromate (BrO_3^-) has garnered plenty of attention in water treatment. In current study, we have developed a novel conjugated donor-acceptor (D-A) photocatalyst (4,4″-bis(diphenylamino)-[1,1′:4′,1″-terphenyl]-2′,5′-dicarbaldehyde, BDTD) with supramolecule architecture assembling via intermolecular C—H···O hydrogen bonds and C—H···π interactions. Both diffuse reflectance spectrum (DRS) and density functional theoretical (DFT) calculations gave the bandgap of E_g = 2.21 eV, clearly indicating the visible-light response of BDTD supramolecule. The calculations showed that BDTD supramolecule could induce nearly 100% removal of BrO_3^- stably at pH-neutral condition driven by visible light, accounting for a first-order kinetic constant being one order of magnitude higher than most of the photocatalysts previous reported. As demonstrated by our electron scavenger experiment and DFT calculations, the BDTD supramolecule should undergo the photocatalytic reduction of BrO_3^- through direct reduced by the lowest unoccupied molecular orbital of conduction band (potential of −1.705 V versus standard hydrogen electrode) electron. The BDTD supramolecule may serve as an attractive photocatalyst by virtue of response to visible light, efficient charge transfer and separation as well as high photocatalytic activity, which will make the removal of BrO_3^- in water much easier, more economical and more sustainable.

* Corresponding author at: P. O. Box 2603#, No. 73, Huanghe Road, Nangang District, Harbin 150090, PR China.
E-mail address: sjyou@hit.edu.cn (S. You).

https://doi.org/10.1016/j.jcis.2019.06.072
0021-9797/

1. Introduction

Over the past decades, there is an increasing concern on bromate (BrO_3^-) produced from the chlorination or ozonation process during treatment of bromide (Br^-)-containing water treatment. Owing to potential carcinogenic and genotoxic risk [1–3], the United States and European countries have set the maximum contaminant level (MCL) of 10 μg L^{-1} for BrO_3^- in drinking water [4–6]. To meet such criterion, several previous studies reported methods to reduce BrO_3^- to innocuous Br^- by using ferrous ions [7], zero-valent iron [8,9] and layered double hydroxides (LDHs) catalyst [10]. However, the engineered applications of these methods may be hindered by their low efficiency, high cost, operational complexity.

Recently, photocatalytic reduction has emerged as a promising method to remove BrO_3^- in water [11], and TiO_2-based semiconductors are the most frequently reported photocatalysts to achieve this goal [12–15]. Excited by ultraviolet (UV) light, the photogenerated electrons (e_{CB}^-) will be produced at conduction band (CB) and photo-generated holes (h_{VB}^+) at valence band (VB). The photo-generated holes are captured by hole trapping agents (electron donors), and the BrO_3^- reduction can be achieved by photogenerated electrons at the CB site [16–19]. Many prior studies have confirmed the vital role of photogenerated electrons during photo-reduction of BrO_3^- [11,14,15]. However, there remain challenges for photo-reduction of BrO_3^- calalyzed by TiO_2-based photocatalysts for several reasons. First, TiO_2 with wide band gap ($E_g \approx$ 3.2 eV) can only be excited by UV light whose spectrum accounts for only 3% in the solar light, which may hamper the engineered applications [15]. Thus, it will be highly desirable to develop photocatalysts that work on visible light (44% of the solar light). Second, there exists limitation for BrO_3^- reduction efficiency due to high valence band potential of TiO_2 that may lead to re-oxidation of Br^- by water oxidation produced ·OH radicals at the VB site [20]. Third, the overall performance may be impaired by the fast recombination of electron-hole pairs, as is often encountered in photocatalytic system [21].

Recently, supramolecular materials have attracted a growing interest since the concept of supramolecular chemistry was first introduced by Wolf et al. in 1937 [22]. The supramolecules represent a class of crystalline organic materials that can be self-assembled by a discrete number of molecular building blocks via non-covalent bond such as hydrogen bonding, van der Waals forces, π-π interactions and electrostatic interaction. This makes it much easier build up desired photo-sensitive supramolecular materials to realize chemical tuning of electronic and optical properties, improving charge separation and electron transfer, as well as widening light response [23–26]. More specifically, the conjugated D-A supramolecule generally exhibits a small band gap that can broaden the response light to the visible and even near-infrared region [27]. The lowest unoccupied molecular orbital (LUMO) can be tuned easily by auxiliary acceptor modification, which is of importance for BrO_3^- reduction in terms of thermodynamic feasibility [28,29]. In addition, the highest occupied molecular orbital (HOMO) and LUMO are separated spatially in D-A systems where an intra-molecular charge transfer facilitates the inner separation of charge carriers. This will largely mitigate the problems of Br^- re-oxidation during BrO_3^- reduction [30,31]. Furthermore, the metal-free supramolecules are more environmentally friendly because of no concern on metal leaching during operation [32]. These features make supramolecular materials suitable for many photochemical applications such as photosensing, photosynthesis, and water splitting. Up to present, however, to our knowledge only few studies have reported on D-A supramolecular photocatalyst for reduction of BrO_3^- in water treatment.

In this study, in order to remove BrO_3^- effectively and stably, we, for the first time, report a novel D-A conjugated supramolecular photocatalyst, *i.e.* 4,4″-bis(diphenylamino)-[1,1′:4′,1″-terphenyl]-2′,5′-dicarbaldehyde (BDTD) for effective reduction of BrO_3^- driven by visible light irradiation. First, the structure and morphology of BDTD supramolecule were acquired on X-ray diffraction (XRD), Fourier transform infrared spectroscopy (FT-IR) and transmission electron microscopy (TEM). Second, the catalytic performance and the cycling stability of BDTD were examined for visible-light-driven reduction of BrO_3^-. Last, the feasible mechanisms associated with electronic configuration for photocatalytic reduction of BrO_3^- by BDTD supramolecule were discussed by using DRS measurement and DFT calculations.

2. Experimental section

All the chemicals used were of analytical reagent grade and purchased from Sigma-Aldrich . The TiO_2 used for photocurrent measurement was commercially available Degussa P25 (Evonik-degussa, Germany).

2.1. Preparation of BDTD supramolecule

The 4,4″-bis(diphenylamino)-[1,1′:4′,1″-terphenyl]- 2′,5′-dicar baldehyde (BDTD) was prepared according to Knoevenagel reaction and Suzuki coupled reaction. In the typical synthesis process, 2,5-dibromoterephthalaldehyde (0.58 g) and (4-(diphenylamino) phenyl)-boronic acid (1.74 g) were added into toluene (50 mL)/tetrahydrofuran (30 mL) solution, and subsequently $Pd(PPh_3)_4$ (0.065 g) and Na_2CO_3 (2.0 mol L^{-1}, 3.0 mL) were poured into the flask. The solution was stirred vigorously at 90 °C under nitrogen atmosphere for 24 h. Next, the solution was extracted by using excessive $CHCl_3$. After purification with a silica gel column, 0.87 g of BDTD could be obtained (yield of 70.1%). ^{1}H NMR (500 MHz, $CDCl_3$): *d* (ppm) 7.11 (t, *J* = 7.5 Hz, 4H); 7.18(d, *J* = 9.0 Hz, 4H); 7.20 (d, *J* = 7.5 Hz, 8H); 7.29(d, *J* = 8.5 Hz, 4H); 7.33(t, *J* = 7.5 Hz, 8H); 8.11(s, 2H); 0.18(s, 2H). 1 ^{13}C NMR (125 MHz, $CDCl_3$): d (ppm) 122.46; 123.74; 125.11; 129.52; 130.15; 130.95; 136.75; 143.87; 147.30; 148.82; 192.15. The synthesis of BDTD supramolecule is schematically illustrated in Fig. 1A.

2.2. Characterization

The powder X-ray diffraction (XRD) characterization was conducted on an X-ray diffractometer (Bruke D8 Adv.; Germany). The UV–Vis diffuse reflectance spectrum (DRS) of BDTD powders were collected using a UV–Vis spectrophotometer (UV-2550, Shimadzu, Japan). The morphologies of samples were observed by using transmission electron microscopy (TEM) and high-resolution TEM (HRTEM) on F-30ST (Tecnai, FEI, US). The functional groups were determined by using Fourier transform infrared spectroscopy (FT-IR; IR Prestige-21, Shimadzu, Japan). The Zeta potential measurement was carried out on a zeta potential analyzer (Nano-Z, Malvern Corp., U.S.) as function of pH. The photocurrent density was measured using an electrochemical workstation (CHI660C, Chenhua Co. Ltd., China) in electrochemical cell containing the working electrode (BDTD), counter electrode, and reference electrode. The working electrode was immersed in sodium bromate electrolyte (0.5 mol L^{-1}) under visible-light irradiation (Xenon lamp, 300 W; CELHXF300, Ceaulight Co. Ltd., China).

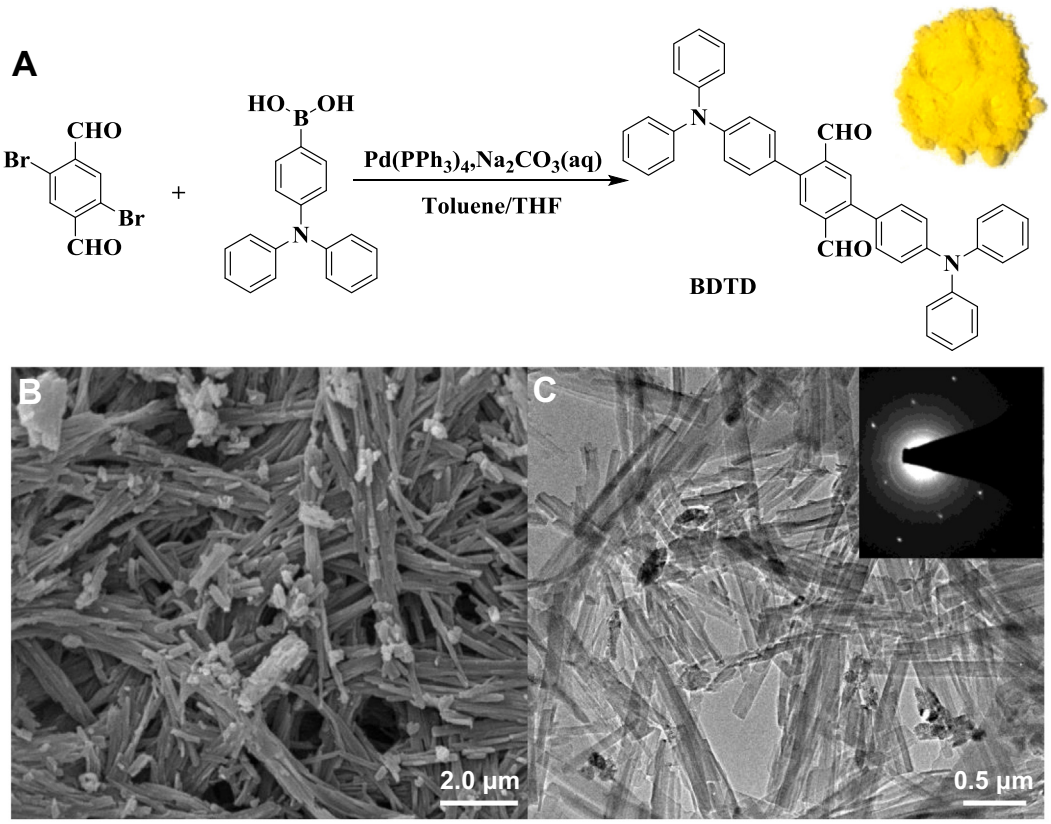

Fig. 1. (A) Synthesis, (B) SEM and (C) TEM image (SAED pattern in inserted figure) of BDTD supramolecule sample.

2.3. Theoretical calculations

The theoretical calculations were conducted by the density functional theory (DFT) package of DMol^3 codes [33]. All electron core treatment was used for all atoms. The self-consistent field (SCF) tolerance was set at 1.0×10^{-5} Ha. Based on the optimized molecular structure, the electronic structure and optical properties could be acquired.

2.4. Experimental setup and procedures

The performances of BDTD for photocatalytic reduction of BrO_3^- ions were examined under visible-light irradiation by employing a Xenon lamp (300 W; CELHXF300, Ceaulight Co. Ltd., China) equipped with a 420 nm cut filter. The average light intensity was approximately 100 mW cm^{-2} on the surface of solution. To overcome kinetic reaction control of the water oxidation reaction, the experiments were conducted with addition of humic acid (HA, Sigma-Aldrich) serving as hole scavenger that interacted with photogenerated hole [20]. In a typical experiment, 0.05 g of BDTD and 0.10 g HA were homogeneously dispersed into 70 mL of BrO_3^- solution (BrO_3-Br, 150 μg L^{-1}, pH 7.1 ± 0.4). Prior to the tests, the adsorption-desorption equilibrium experiment was first implemented, and the corresponding data can be found in Table S1, the catalyst with the adsorption-desorption equilibrium was added to a fresh solution (BrO_3-Br, 150 μg L^{-1}). Then, the mixed solution was exposed to visible light irradiation at a reaction time of 40 min (degradation experiment was carried out in 60 min, and the degradation rate is stable after 25 min). The liquid samples were withdrawn at given time intervals for analysis after centrifugation at 8000 rpm (7155*g*) and filtration using 0.2 μm cellulose acetate membrane. Both BrO_3^- and Br^- ions were determined by using ion chromatograph analyzer (LC-10A, Shimadzu, Japan).

3. Results and discussion

3.1. Characterization of BDTD supramolecule

As shown in Fig. 1A, the BDTD supramolecule contains the benzene ring attached to two aldehyde groups in the central part and twisty triphenylamine structures at the two ends in its molecular model. The as-prepared BDTD supramolecule samples are dark yellow powders. Both SEM (Fig. 1B) and TEM image (Fig. 1C) illustrates the long-strip shaped clusters with the length of 3–6 μm and width of 100 nm for the individuals. The inserted HRTEM image of selected area electron diffraction (SAED) demonstrates the regular rhombus single crystalline diffraction spots, indicating the single crystals of BDTD aggregation growing along longitudinal direction. The crystalline nature of BDTD supramolecule can be further confirmed by the XRD pattern (Fig. 2A), showing sharp and intense diffraction peaks as function of 2θ. This information reflected the high crystallinity of BDTD aggregation assembling via supramolecule interaction rather than amorphous polymerization. Both experimental and calculated FT-IR data (Table S2 and Fig. 2B) give the characteristic bands at wavenumber of 1590 and 1428 cm^{-1} originating from the stretching modes of C=C in aromatic rings. The peak at 695 cm^{-1} should be caused by the stretching of C=O in the benzene ring (aliphatic aldehyde) [34–36]. The in-plane bending vibration of aliphatic aldehyde at ellipse callout area appeared stronger than that of BDTD monomer, suggesting the BDTD supramolecular aggregation occurring at the C=O position of the benzene ring via the conjugated C—H···O hydrogen bonds and C—H···π interactions [37–39]. As shown in Fig. 3C, the UV–Vis absorption spectrum revealed the absorption band edge of wavelength of λ = 560 nm, which corresponded to the band gap of E_g = 2.21 eV according to $E_g = 1240/\lambda$ [40,41]. This clearly suggested the response of visible light for BDTD supramolecule

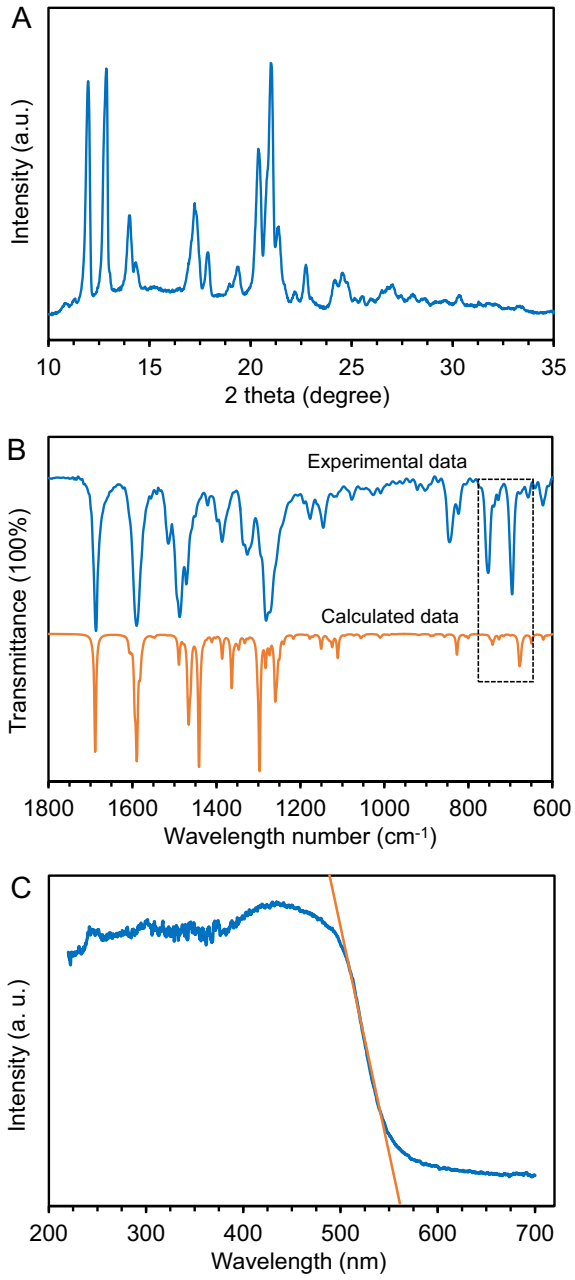

Fig. 2. (A) XRD pattern, (B) DRS spectra, and (C) FT-IR spectra of BDTD supramolecule.

material. Compared with BDTD monomer, the formation of supramolecule structure could widen the range of light response edge toward the visible light from 485 nm (E_g = 2.56 eV) to 560 nm (E_g = 2.21 eV; Fig. S1).

3.2. Photocatalytic Reduction of BrO_3^- by BDTD Supramolecule

We examined the feasibility of using BDTD supramolecule for photocatalytically reducing BrO_3^- (initial concentration of 150 μg L^{-1} and pH 7.1 ± 0.4) when the humic acid (HA) serving as the scavenger under visible light irradiation. No BrO_3^- reduction was observed in the absence of photocatalyst (control experiment), indicate that no direct redox reaction between BrO_3^- and HA. As illustrated in Fig. 3A, the BDTD supramolecule was able to remove BrO_3-Br concentration from initial 150 μg L^{-1} to 0 μg L^{-1} at 40 min, which accounted for almost 100% BrO_3^- reduction. The BrO_3^- removal agreed well with a first-order kinetics with constant of 0.1533 min^{-1} (Table S3). Meanwhile, as shown in Fig. 3A and Table S4, the BrO_3-Br was almost reduced to Br^- during the photocatalytic reduction process, and more than 96% BrO_3^- was converted to Br^- at the end of reaction, this indicate the BDTD supramolecule catalyst can reduced BrO_3-Br to Br^- effectively in aqueous solution driven by visible light.

Next, we further investigated the effect of photocatalyst dosage, initial BrO_3^- concentration and pH on BrO_3^- removal. As illustrated in Fig. 3B, the residual concentration BrO_3^- was observed to increase from 0 μg L^{-1} (removed by 100%) to 57.0 μg L^{-1} (removed by 62%) when decreasing the concentration of BDTD supramolecule powders from 0.10 to 0.02 g. The positive correlation between catalyst dosage and BrO_3^- removal suggested the significant role of BDTD supramolecule because higher dosage of catalyst could provide more active sites for BrO_3^- reduction. On the other hand, the photocatalytic efficiency also depended on the initial concentration of BrO_3^- in solution. For example, the kinetic constant decreased from 0.1533 to 0.0752 min^{-1} when initial BrO_3-Br concentration was increased from 50 to 300 μg L^{-1} (Fig. 3C and Table S5). Notably, the photocatalytic reaction of BDTD supramolecule was found to be highly pH-dependent, *i. e.* the BrO_3^- reduction was optimized at pH-neutral condition, yet inhibited remarkably under both acidic and alkaline condition (Fig. 3D and Table S6). Such phenomenon appeared to be quite attractive because it eliminated the need for pH adjustment (assuming initial pH is typically ~ 7.0), making it much favorable in engineered applications.

To elucidate the pH-dependent behavior of BDTD supramolecule, we investigated the zeta potential at various pH values. As shown in Fig. S2, the stepwise change of pH from 1.0 to 11.0 led to a decrease in zeta potential from +27.15 mV to −24.32 mV. The intercept of zeta potential curve and *x*-axis gave an isoelectric point (IEP) of approximately pH 6.4, suggesting the amphoteric nature of BDTD supramolecule. The zeta potential was shifted to the regions that were more electrically positive for lower pH and negative for higher pH. The positive shift at pH lower than IEP should be the consequence of the protonation of functional groups (*i. e.* carbonyl groups) on the surface of BDTD supramolecule. In this case, the electrostatic attraction between protons and BrO_3^- had driven the transfer and adsorption of BrO_3^- ions onto the protonated surface of the photocatalyst. Conversely, the inherent electrostatic repulsion could take place at pH higher than IEP, which resulted in prevention of BrO_3^- adsorbing on the negatively charged surface of triphenylamine groups. This should be the most likely reason for higher BrO_3^- removal observed under acidic condition than that obtained under alkaline conditions. Nevertheless, lower pH could also increase the consumption of OH^- and thus promote the formation of $HO_2^{\cdot}$ radicals, the oxidative species that might react with Br^- to form BrO_3^- again [42]. This could provide the most probable explanation to the highest BrO_3^- removal at pH values being close to IEP for BDTD supramolecule.

The stability of BDTD supramolecule was evaluated by performing the experiments of catalyst recycling. After each running cycle, the BDTD powders were recycled by washing with DI-water and absolute ethanol, and then re-tested under the same conditions as before. As documented in Fig. S3, there was almost no observation of decrease in photocatalytic activity and BrO_3^- removal (100%) during the four-cycle consecutive experiments, suggesting a good stability of BDTD supramolecule during photocatalytic reduction of BrO_3^- in water.

3.3. Mechanisms

During the bromate reduction process, the bromate may be reduced by (i) reductive $CO_2^{\cdot-}$ radicals through the hole scavengers oxidation reaction and (ii) the photo-generated electrons. The

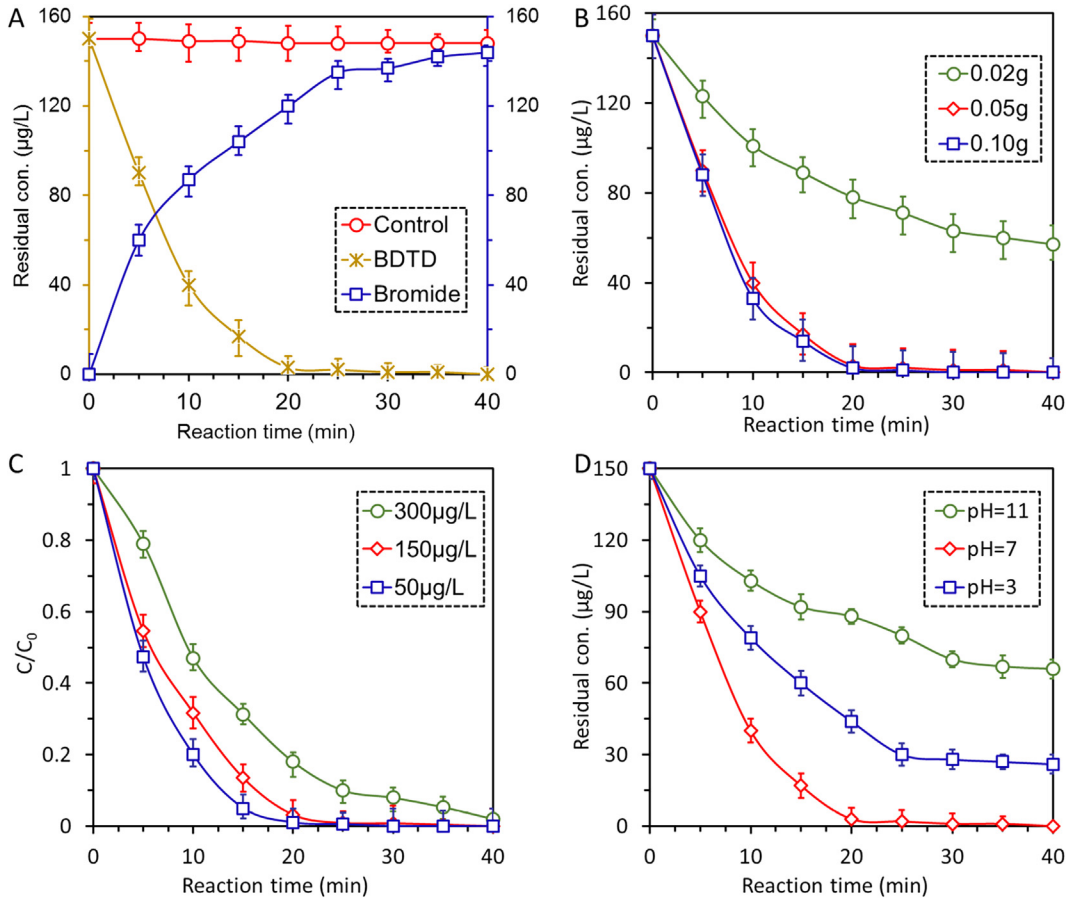

Fig. 3. Time course of (A) photocatalytic reduction of BrO_3^- by BDTD supramolecule under visible light irradiation at pH 7.1 ± 0.4, effect of (B) catalyst dosage, (C) initial BrO_3^- concentration, and (D) pH values on BrO_3^- removal. The error bars ± S.D. indicate the measurements in triplicate.

organic sacrificial agent such as Formic Acid (FA) is a common hole scavenger to produce $CO_2^{\cdot-}$ radicals. To identify the role of $CO_2^{\cdot-}$ radicals in the current experiment, we performed the experiments by choosing four types scavengers (organic and inorganic hole scavengers), *i.e.* HA, FA, Na_2SO_3 and ascorbic acid (AA). As shown in Table 1, there has no obvious difference on the bromate reduction efficiency between these four hole scavengers. BDTD achieved high bromate reduction efficiency without a dependency on hole scavengers, especially when use of the inorganic reagent Na_2SO_3 as hole scavenger, the kinetic constant responsible for BrO_3^- reduction is 0.1287 min^{-1}, which indicates that Na_2SO_3 has a negligible impact on BrO_3^- reduction compare with HA. Note that HA is the common natural organic matter (NOM) in natural water [43], this indicates a technological opportunity of using humic substances or NOM present natural water matrix to accompany *on-site* BrO_3^- reduction eliminating the addition any hole scavenger. Based on the experimental result, we draw a conclusion that the bromate reduction by BDTD supramolecule should be dominated by the reactions involving the CB via interaction with photo-generated electrons.

Table 1
Effect of a Hole Scavenger on BrO_3^- reduction and Br^- selectivity.

Scavenger	Kinetic constant	Br^- selectivity
HA	0.1533 min^{-1}	96%
Na_2SO_3	0.1287 min^{-1}	92%
AA	0.1640 min^{-1}	95%
FA	0.1387 min^{-1}	90%

The DFT calculations indicated that the HOMO and LUMO were located on the donor (−5.125 eV) and acceptor (−2.895 eV) site, respectively, forming the conjugated D-A structure in the BDTD supramolecule. The calculated bandgap of 2.23 eV was in good agreement with that obtained from DRS measurement. The E_{VB} and E_{CB} could be estimated according to [44]

$$E_{VB} = -E_{HOMO} - 4.6 \quad (1)$$

$$E_g = E_{VB} - E_{CB} \quad (2)$$

Eqs. (1) and (2) gave the E_{VB} of +0.525 V vs standard hydrogen electrode, SHE and E_{CB} of −1.705 V vs SHE, respectively. The potential for reduction of BrO_3^- was calculated to be $E(BrO_3^-/Br^-)$ = 1.01 V at pH = 7.0 by using Nernst equation [45]. This clearly suggested that the reduction of BrO_3^- to Br^- was thermodynamically favorable driven by e_{CB} of BDTD supramolecule. By plotting the molecular structure of BDTD, it can be seen that the HOMO and LUMO were separated spatially. The HOMO is localized solely on the triphenylamine linker unit, whereas the LUMO is delocalized across the conjugated C—H···O hydrogen bonds and C—H···π interactions. When associating the HOMO with the charge-transfer sites for holes, we may speculate that efficient hole quenching is possible through the direct interactions with the sacrificial donor (HA) via the triphenylamine groups, and the electrons of the delocalized LUMO site across conjugated C—H···O hydrogen bonds and C—H···π interactions are responsible for reducing target electron acceptor BrO_3^-. On the other hand, the E_{VB} value (+0.525 V) is far lower than the potential for water oxidation to produce reactive oxidative species like ·OH radicals (+2.8 V) [46], and thus it appeared unlikely for

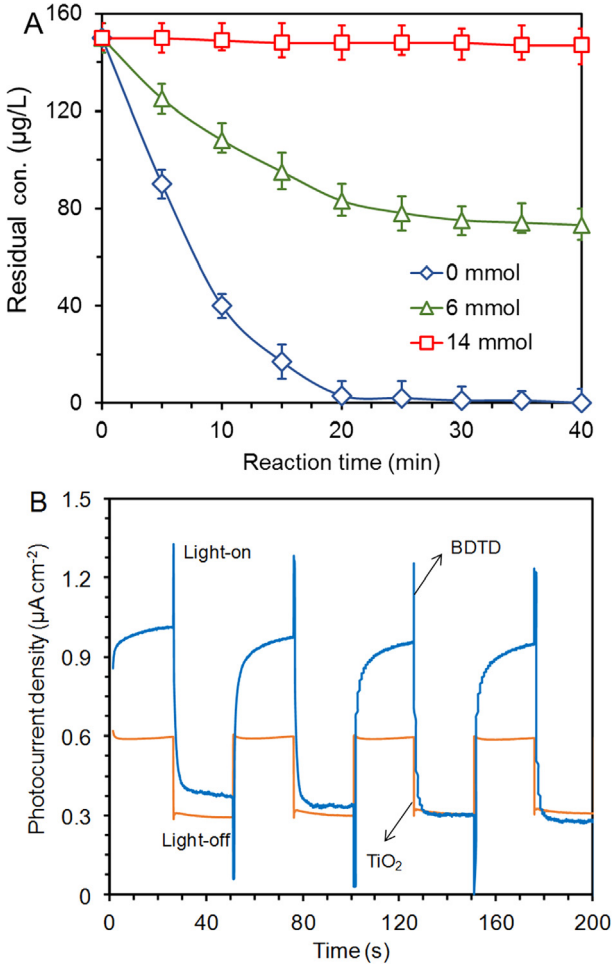

Fig. 4. (A) Effect of electron scavenger $K_2S_2O_8$ on photocatalytic reduction of BrO_3^- (pH 7.1 ± 0.4), and (B) visible-light photocurrent density of BDTD supramolecule and TiO_2 (P25) measured in 0.5 mol L^{-1} $NaBrO_3$ electrolyte. The error bars represent measurements in triplicate.

Br^- to be re-oxidized back to BrO_3^- by ·OH radicals in this system. This may provide one most likely explanation to the reason for effective reduction of BrO_3^- by BDTD supramolecule under visible light irradiation.

To further verify the direct reduction of BrO_3^- by electrons on BDTD supramolecule, electron quenching experiments were carried out by selecting $S_2O_8^{2-}$ as specific electron scavenger because of its much higher thermodynamic selectivity toward electrons (the redox potential of +2.01 V vs SHE at pH 7.0) than BrO_3^- (+1.482 V) [47–50]. The introduction of $S_2O_8^{2-}$ was found to considerably inhibit the BrO_3^- removal, and the extent of inhibition was positively correlated with the amount of $S_2O_8^{2-}$ (Fig. 4A and Table S7) Notably, the photocatalytic activity of BDTD supramolecule toward BrO_3^- reduction nearly disappeared (removed by only ca. 4.0%) when 14 mmol $K_2S_2O_8$ was added. In other words, the addition of $S_2O_8^{2-}$ impeded the electron transfer toward BrO_3^-. Thus, it could be inferred that the BDTD supramolecule proceeded with photocatalytic reduction of BrO_3^- attributable to direct reduction by photo-generated electron. The possible mechanisms are schematically illustrated in Fig. 5.

Another advantage of conjugated D-A architecture for BDTD supramolecule is the more efficient electron transfer and electron/hole separation. Under visible light irradiation, the peak photocurrent density (a higher photocurrent density imply a higher carrier separation efficiency) for BDTD supramolecule (1.0 μA cm^{-2}) was much larger than that for TiO_2 (P25; 0.6 μA cm^{-2}), suggesting faster electron transfer and higher electron-hole separation efficiency [51,52]. This may originate from the inherent spatially separated VB and CB in conjugated D-A structure. Besides, the observation of charging-discharging sharp spikes at switchable light on/off points for BDTD supramolecule in Fig. 4B, indicating the capacitive current associated with adsorption of reactive species (BrO_3^-) on the surface of photocatalyst [53,54].

4. Applications and implications

Recently, photocatalytic reduction has attracted increasing attention as a promising method to remove BrO_3^- in water. Although the feasibility of TiO_2-based photocatalysts have been

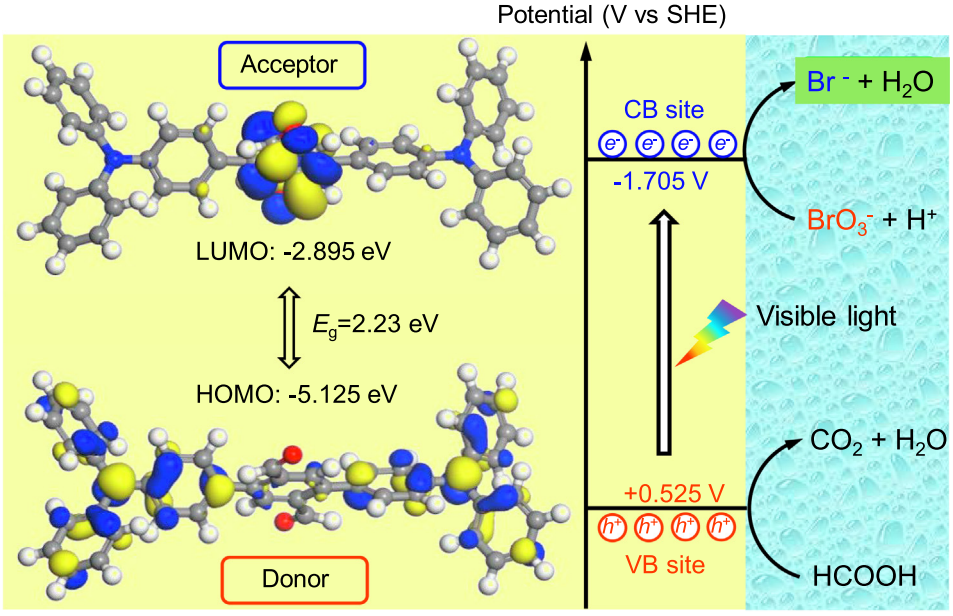

Fig. 5. Schematic illustration of visible-light-driven photocatalytic reduction of BrO_3^- by BDTD supramolecule.

Table 2
Comparison of photocatalytic reduction of BrO_3^- for different photocatalysts.

Photocatalyst	$[BrO_3^-]_0$ and pH	Kinetic constant (min^{-1})	Light source	Reference
Graphene-TiO_2 (Degussa P25, 0.1 g L^{-1})	10 mg L^{-1}; pH = 5.1–9.2	0.0094–0.021	UV, λ = 254 nm; 20 mW cm^{-2}	[42]
0.4 g L^{-1}Pt/TiO_2	50 μg L^{-1}; pH = 8.1	0.0093	UV, λ = 254 nm; 15 mW cm^{-2}	[55]
0.2 g L^{-1} Pseudo-BM/TiO_2	200 μg L^{-1}; pH = 7	0.0041–0.0092	UV, λ = 254 nm; 0.5 mW cm^{-2}	[12]
0.5 g L^{-1} TiO_2 (Degussa P25)	0.1 mmol L^{-1}; pH 1.5–13.5	0.0062	UV, λ = 365 nm; 1150 mW cm^{-2}	[56]
0.5 g L^{-1} Ag@RGO@$BiVO_4$	150 μg L^{-1}; pH = 3–11	0.015–0.117	Visible light, λ > 420 nm; 100 mW cm^{-2}	[1]
0.83 g L^{-1} C_{60}/Bi_2MoO_6	30 μg L^{-1}; pH = 7	0.0034–0.010	Visible light, λ > 420 nm; 500 W Xe lamp	[57]
0.83 g L^{-1} BDTD supramolecule	150 μg L^{-1}; pH = 7	0.1533	Visible light, λ > 420 nm; 100 mW cm^{-2}	This study

reported in many previous studies, there remain several challenges associated with low reduction efficiency due to re-oxidation of Br^- by ·OH radicals at valence band, the response of narrow light spectrum (*i. e.* UV light), and recombination of electrons and holes. To address these problems, we herein developed a novel conjugated donor-acceptor (D-A) supramolecule photocatalyst (BDTD) and demonstrated effective removal of BrO_3^- driven by visible light. The BDTD supramolecule could achieve nearly 100% removal of BrO_3^- at pH-neutral condition, in correspondence to the kinetic constants much higher than most of results obtained with TiO_2, $BiVO_4$, Bi_2MoO_6 in previously reported literatures as documented in Table 2.

In light of the above results, the present study provides the first demonstration of supramolecule material to design photocatalyic system toward BrO_3^- removal for water treatment. The conjugated D-A structured BDTD supramolecule contains spatially separated HOMO and LUMO located on donor and acceptor site, respectively. Compared with BDTD monomer, the formation of supramolecule structure via conjugated C—H···O hydrogen bonds and C—H···π interactions widens the range of light response. As revealed from both experimental results and theoretical calculations, the band-gap of E_g = 2.3 eV indicates the capability of BDTD to response within the spectrum of visible light. This makes the BrO_3^- removal much easier, more economical and more sustainable. The LUMO site having a potential of E_{CB} = −1.705 V vs SHE enables the direct reduction of target electron acceptor BrO_3^- by electrons at conduction band, whilst the low E_{VB} level (+0.525 V vs SHE) excludes the possibility of re-oxidation of Br^-. In addition, the spatially separated D-A structure allows efficient charge transfer and separation, high visible-light photocatalytic performance and good stability toward reduction of BrO_3^-. Moreover, it is also possible to individually tune the LUMO level at acceptor site by inserting an auxiliary acceptor for improved electron trapping. These properties make the BDTD supramolecule particularly attractive for BrO_3^- removing in water treatment. In future work, it will be necessary to continue the investigations on interference with complex electron donors such as natural organic matter (NOM) or effluent organic matters and co-existing anions, and develop the visible-light photocatalytic process for more practical applications.

5. Conclusions

In this study, the bromate was photocatalytic reduced by well-defined D-A supramolecule photocatalyst under visible light. At pH-neutral and visible light irradiation conditions, the D-A supramolecule BDTD photocatalyst can degradation of bromate to bromide effectively and stably with a first-order kinetic constant of 0.1533 min^{-1}. As indicated by DRS, photocurrent measurements and DFT calculations, the electronic configuration of BDTD photocatalyst (D-A structure) made it with low CB position (E_{CB} = −1.705 V), high carrier separation efficiency, and good stability, all of these properties should be accountable for removal of bromate in photocatalytic reduction process. This investigation provided a simple and effective strategy for enhanced degradation of bromate without need for chemical addition and pH adjustment, making bromate removal more efficient and more sustainable, and give a guideline for the development of supramolecule catalyst for bromate photocatalytic reduction.

Acknowledgements

Project supported by the National Natural Science Foundation of China (Grant No. 51822806, 51678184, 51761145031) and "Fundamental Research Funds for the Central Universities" (Grant No. HIT.BRETIV.201905). The authors thank the China Scholarship Council for supporting our work (No. 201806120344).

Appendix A. Supplementary material

Supplementary data to this article can be found online at https://doi.org/10.1016/j.jcis.2019.06.072.

References

[1] F. Chen, Q. Yang, Y. Zhong, H. An, J. Zhao, T. Xie, Q. Xu, X. Li, D. Wang, G. Zeng, Photo-reduction of bromate in drinking water by metallic Ag and reduced graphene oxide (RGO) jointly modified $BiVO_4$ under visible light irradiation, Water Res. 101 (2016) 555–563.
[2] K.M. Parker, T. Zeng, J. Harkness, A. Vengosh, W.A. Mitch, Enhanced formation of disinfection byproducts in shale gas wastewater-impacted drinking water supplies, Environ. Sci. Technol. 48 (2014) 11161–11169.
[3] S. Bouland, J.-P. Duguet, A. Montiel, Evaluation of bromate ions level introduced by sodium hypochlorite during post-disinfection of drinking water, Environ. Technol. 26 (2005) 121–126.
[4] X. Wu, Q. Yang, D. Xu, Y. Zhong, K. Luo, X. Li, H. Chen, G. Zeng, Simultaneous adsorption/reduction of bromate by nanoscale zerovalent iron supported on modified activated carbon, Ind. Eng. Chem. Res. 52 (2013) 12574–12581.
[5] H.S. Weinberg, C.A. Delcomyn, V. Unnam, Bromate in chlorinated drinking waters: occurrence and implications for future regulation, Environ. Sci. Technol. 37 (2003) 3104–3110.
[6] M.L. Bao, O. Griffini, D. Santianni, K. Barbieri, D. Burrini, F. Pantani, Removal of bromate ion from water using granular activated carbon, Water Rese. 33 (1999) 2959–2970.
[7] W. Shen, F. Lin, X. Jiang, H. Li, Z. Ai, L. Zhang, Efficient removal of bromate with core-shell Fe@Fe_2O_3 nanowires, Chem. Eng. J. 308 (2017) 880–888.
[8] L. Xie, C. Shang, The effects of operational parameters and common anions on the reactivity of zero-valent iron in bromate reduction, Chemosphere 66 (2007) 1652–1659.
[9] Q. Wang, S. Snyder, J. Kim, H. Choi, Aqueous ethanol modified nanoscale zerovalent iron in bromate reduction: synthesis, characterization, and reactivity, Environ. Sci. Technol. 43 (2009) 3292–3299.
[10] Y. Zhang, S. Jing, H. Liu, Reactivity and mechanism of bromate reduction from aqueous solution using Zn–Fe (II)–Al layered double hydroxides, Chem. Eng. J. 266 (2015) 21–27.
[11] Z. Yan, L. Li, H. Liu, Photocatalytic reduction activity of 001 TiO2 co-doped with F and Fe under visible light for bromate removal, J. Nanomater. (2016, (2016–11-24) 2016, 2016,) 1–7.
[12] H. Noguchi, A. Nakajima, T. Watanabe, K. Hashimoto, Removal of bromate ion from water using TiO_2 and alumina-loaded TiO_2 photocatalysts, Water Sci. Technol. 46 (2002) 27–31.
[13] D. Chongxiong, H. Jinhao, L. Feier, Y. Minhui, X. Hongxia, Ultrafast room-temperature synthesis of hierarchically porous metal–organic frameworks by a versatile cooperative template strategy, J. Mater. Sci. 53 (2018) 16276–16287.
[14] K.Y.A. Lin, C.H. Lin, S.Y. Chen, H. Yang, Enhanced photocatalytic reduction of concentrated bromate in the presence of alcohols, Chem. Eng. J. 303 (2016) 596–603.
[15] N. Hiroshi, N. Akira, W. Toshiya, H. Kazuhito, Design of a photocatalyst for bromate decomposition: surface modification of TiO_2 by pseudo-boehmite, Environ. Sci. Technol. 37 (2003) 153–157.

[16] F. Zhang, R. Jin, J. Chen, C. Shao, W. Gao, L. Li, N. Guan, High photocatalytic activity and selectivity for nitrogen in nitrate reduction on Ag/TiO_2 catalyst with fine silver clusters, J. Catal. 232 (2005) 424–431.
[17] A. Sadeghzadeh-Attar, Efficient photocatalytic degradation of methylene blue dye by SnO_2 nanotubes synthesized at different calcination temperatures, Sol. Energ. Mat. Sol. C. 183 (2018) 16–24.
[18] J. Zhang, Y. Gao, X. Jia, J. Wang, Z. Chen, Y. Xu, Oxygen vacancy-rich mesoporous ZrO_2 with remarkably enhanced visible-light photocatalytic performance, Sol. Energ. Mat. Sol. C. 182 (2018) 113–120.
[19] Y. Wu, Y. Wei, Q. Guo, H. Xu, L. Gu, F. Huang, D. Luo, Y. Huang, L. Fan, J. Wu, Solvothermal fabrication of La-WO_3/$SrTiO_3$ heterojunction with high photocatalytic performance under visible light irradiation, Sol. Energ. Mat. Sol. C. 176 (2018) 230–238.
[20] G. Liu, S. You, M. Ma, H. Huang, N. Ren, Removal of nitrate by photocatalytic denitrification using nonlinear optical material, Environ. Sci. Technol. 50 (2016) 11218–11225.
[21] X. Li, Y. Pi, Q. Xia, L. Zhong, X. Jing, TiO_2 encapsulated in Salicylaldehyde-NH_2-MIL-101(Cr) for enhanced visible light-driven photodegradation of MB, Appl. Catal. B Environ. 191 (2016) 192–201.
[22] K. Wolf, H. Frahm, H. Harms, The state of arrangement of molecules in liquids, Z. Phys. Chem. Abt. B 36 (1937) 237–287.
[23] J.J. Perry, J.A. Perman, M.J. Zaworotko, Design and synthesis of metal-organic frameworks using metal-organic polyhedra as supermolecular building blocks, Chem. Soc. Rev. 38 (2009) 1400–1417.
[24] N. Farid, J.F. Eubank, B. Till, W. Lukasz, M.J. Zaworotko, E. Mohamed, Supermolecular building blocks (SBBs) for the design and synthesis of highly porous metal-organic frameworks, J. Am. Chem. Soc. 130 (2008) 1833–1835.
[25] G. Vincent, K. Dongwook, J.F. Eubank, L. Ryan, L. Xinfang, A. Karim, L. Myoung Soo, E. Mohamed, A supermolecular building approach for the design and construction of metal-organic frameworks, Chem. Soc. Rev. 45 (2015) 6141–6172.
[26] Z. Zhang, L. Wojtas, M.J. Zaworotko, Organic–inorganic hybrid polyhedra that can serve as supermolecular building blocks, Chem. Sci. 5 (2014) 927–931.
[27] J.-L. Brédas, D. Beljonne, V. Coropceanu, J. Cornil, Charge-transfer and energy-transfer processes in π-conjugated oligomers and polymers: a molecular picture, Chem. Rev. 104 (2004) 4971–5004.
[28] G. Yu, J. Gao, J.C. Hummelen, F. Wudl, A.J. Heeger, Polymer Photovoltaic Cells: Enhanced Efficiencies via a Network of Internal Donor-Acceptor Heterojunctions, Science 270 (1995) 1789–1791.
[29] S. Ahmad, E. Guillén, L. Kavan, M. Grätzel, M.K. Nazeeruddin, Metal free sensitizer and catalyst for dye sensitized solar cells, Energ. Environ. Sci. 6 (2013) 3439–3466.
[30] S.R. Jakob Kryger, V. Mikkel, K. Anders, K. Kristine, Synthesis of oligo (phenyleneethynylene)-tetrathiafulvalene cruciforms for molecular electronics, Org. Lett. 8 (2006) 1173–1176.
[31] A.J. Zucchero, P.L. Mcgrier, U.H. Bunz, Cross-conjugated cruciform fluorophores, Accounts Chem. Res. 43 (2010) 397–408.
[32] C.Z. Hai, E.Q. Guo, L.Z. Yan, H.R. Pei, J.Y. Wen, Donor−acceptor-substituted anthracene-centered cruciforms: synthesis, enhanced two-photon absorptions, and spatially separated frontier molecular orbitals, Chem. Mater. 21 (2009) 5125–5135.
[33] B. Delley, From molecules to solids with the DMol3 approach, J. Chem. Phy. 113 (2000) 7756–7764.
[34] V. Manivannan, N. Vembu, M. Nallu, K. Sivakumar, F.R. Fronczek, Phenyl 4-toluenesulfonate: Supramolecular aggregation through weak C-H···O and C-H···π interactions, Acta Crys. C 61 (2005) o2736–o2738.
[35] G. Blanco-Brieva, M.C. Capel-Sanchez, J.M. Campos-Martin, J.L.G. Fierro, Effect of precursor nature on the behavior of titanium-polysiloxane homogeneous catalysts in primary alkene epoxidation, J. Mol. Catal. A Chem. 269 (2007) 133–140.
[36] G. Lalwani, A.T. Kwaczala, S. Kanakia, S.C. Patel, S. Judex, B. Sitharaman, Fabrication and characterization of three-dimensional macroscopic all-carbon scaffolds, Carbon 53 (2013) 90–100.
[37] Y. Li, F. Li, H. Zhang, Z. Xie, W. Xie, H. Xu, B. Li, F. Shen, L. Ye, M. Hanif, Tight intermolecular packing through supramolecular interactions in crystals of cyano substituted oligo(para-phenylene vinylene): a key factor for aggregation-induced emission, Chem. Comm. 3 (2007) 231–233.
[38] H.H. Fang, Q.D. Chen, J. Yang, H. Xia, B.R. Gao, J. Feng, Y.G. Ma, H.B. Sun, Two-photon pumped amplified spontaneous emission from cyano-substituted oligo (p-phenylenevinylene) crystals with aggregation-induced emission enhancement, J. Phy. Chem. C 114 (2010) 11958–11961.
[39] H. Wang, F. Li, I. Ravia, B. Gao, Y. Li, V. Medvedev, H. Sun, N. Tessler, Y. Ma, Cyano-substituted oligo (p-phenylene vinylene) single crystals: a promising laser material, Adva. Funct. Mater. 21 (2011) 3770–3777.
[40] G. Liu, S. Liu, Q. Lu, H. Sun, Z. Xiu, Synthesis of mesoporous $BiPO_4$ nanofibers by electrospinning with enhanced photocatalytic performances, Ind. Eng. Chem. Res. 53 (2014) 13023–13029.
[41] P. Chengsi, Z. Yongfa, New type of $BiPO_4$ oxy-acid salt photocatalyst with high photocatalytic activity on degradation of dye, Environ. Sci. Technol. 44 (2010) 5570–5574.
[42] X. Huang, L. Wang, J. Zhou, N. Gao, Photocatalytic decomposition of bromate ion by the UV/P25-Graphene processes, Water Res. 57 (2014) 1–7.
[43] C. Jiang, B.T. Castellon, C.W. Matson, G.R. Aiken, H. Hsu-Kim, Relative contributions of copper oxide nanoparticles and dissolved copper to cu uptake kinetics of gulf killifish (fundulus grandis) embryos, Environ. Sci. Technol. 51 (2017) 1395–1404.
[44] S. Kera, H. Yamane, H. Honda, H. Fukagawa, K.K. Okudaira, N. Ueno, Photoelectron fine structures of uppermost valence band for well-characterized ClAl-phthalocyanine ultrathin film: UPS and MAES study, Surf. Sci. 566 (2004) 571–578.
[45] H. Chen, Z. Xu, H. Wan, J. Zheng, D. Yin, S. Zheng, Aqueous bromate reduction by catalytic hydrogenation over Pd/Al_2O_3 catalysts, Appl. Catal. B Environ. 96 (2010) 307–313.
[46] R. Yuan, S.N. Ramjaun, Z. Wang, J. Liu, Effects of chloride ion on degradation of acid orange 7 by sulfate radical-based advanced oxidation process: Implications for formation of chlorinated aromatic compounds, J. Hazard. Mater. 196 (2011) 173–179.
[47] I. Grčić, D. Vujević, N. Koprivanac, Modeling the mineralization and discoloration in colored systems by (US)Fe^{2+}/H_2O_2 /$S_2O_8^{2-}$ processes: A proposed degradation pathway, Chem. Eng. J. 157 (2010) 35–44.
[48] X.Y. Chen, R.J. Zheng, S.F. Qin, J.J. Sun, Hot electron-induced cathodic electrochemiluminescence at oil film-covered carbon paste electrode and application to nano-molar determination of catechol, Talanta 101 (2012) 362–367.
[49] S. Kundu, A. Kafizas, G. Hyett, A. Mills, J.A. Darr, I.P. Parkin, An investigation into the effect of thickness of titanium dioxide and gold–silver nanoparticle titanium dioxide composite thin-films on photocatalytic activity and photo-induced oxygen production in a sacrificial system, J. Mater. Chem. 21 (2011) 6854–6863.
[50] S. Biswas, Robust mesoporous manganese oxide catalysts for water oxidation, ACS Catal. 5 (2015) 1693–1699.
[51] G. Liu, S. You, Y. Tan, N. Ren, In situ photochemical activation of sulfate for enhanced degradation of organic pollutants in water, Environ. Sci. Technol. 51 (2017) 2339–2346.
[52] Y. Zhu, J. Ren, X. Yang, G. Chang, Y. Bu, G. Wei, W. Han, D. Yang, Interface engineering of 3D $BiVO_4$/Fe-based layered double hydroxide core/shell nanostructures for boosting photoelectrochemical water oxidation, J. Mater. Chem. A 5 (2017) 9952–9959.
[53] M.C. Long, W.M. Cai, H. Kisch, Visible light induced photoelectrochemical properties of n-$BiVO_4$ and n-$BiVO_4$/pCo_3O_4, J. Phy. Chem. C 112 (2008) 548–554.
[54] M. Hebda, G. Stochel, K. Szaciłowski, W. Macyk, Optoelectronic switches based on wide band gap semiconductors, J. Phy. Chem. B 110 (2006) 15275–15283.
[55] A. Mills, A. Belghazi, D. Rodman, Bromate removal from drinking water by semiconductor photocatalysis, Water Res. 30 (1996) 1973–1978.
[56] X. Zhang, T. Zhang, J. Ng, J.H. Pan, D.D. Sun, Transformation of bromine species in TiO_2 photocatalytic system, Environ. Sci. Technol. 44 (2009) 439–444.
[57] X. Zhao, H.J. Liu, Y.L. Shen, J.H. Qu, Photocatalytic reduction of bromate at C_{60} modified Bi_2MoO_6 under visible light irradiation, Appl. Catal. B Environ. 106 (2011) 63–68.